



Determination of the number of components in the PARAFAC model with a nonnegative tensor structure: a simulated EEG data study

Zuzana Rošťáková¹ · Roman Rosipal^{1,2}

Received: 17 January 2022 / Accepted: 18 April 2022

© The Author(s), under exclusive licence to Springer-Verlag London Ltd., part of Springer Nature 2022

Abstract

Parallel factor analysis (PARAFAC) is a powerful tool for detecting latent components in human electroencephalogram (EEG) in the time-space-frequency domain. As an essential parameter, the number of latent components should be set in advance. However, any component number selection method already proposed in the literature became a rule of thumb. Existing studies have demonstrated the methods' performance on artificial data with a simplified structure, often not mimicking a real data character. On the other hand, the ground-truth latent structure is not always known for real-world data. With the objective to provide a comprehensive overview of component number selection methods and discuss their applicability to EEG, our study focuses on nontrivial and nonnegative simulated data structures resembling real EEG properties as closely as possible. This is achieved through an accurate head model and well-controlled cortical activation sources. By considering different noise levels and disruptions from the optimal structure, the performance of the twelve component number selection methods is closely inspected. Moreover, we validate a new approach for component number selection, which we recently proposed and applied to EEG tasks. We found that methods based on the eigenvalue analysis, variance explained, or presence of redundant components are inappropriate for component number selection in EEG tensor decomposition. On the other hand, three existing methods and the newly proposed approach produced promising results on nontrivial simulated EEG data. Nevertheless, component number selection for PARAFAC analysis of EEG is a complex yet unresolved problem, and new approaches are needed.

Keywords Parallel factor analysis · Component number selection · Simulated electroencephalogram

1 Introduction

Real data represent complex phenomena that often combine correlated measured variables generated or determined by unobservable latent components. To better understand the recorded data structure or to represent such data in a parsimonious low-rank format, we often focus on

identifying and extracting these latent components [1]. A widely used tool for this purpose represents a set of data factorization methods, including principal component analysis (PCA), independent component analysis (ICA), and nonnegative matrix factorization [1]. These methods have been studied for a long time, and their mathematical and convergence properties are well known. These methods are based on the representation of data in the form of a matrix, where measured variables are represented by one dimension (modality) and repeated recordings (samples) by the other.

However, we often observe and record and analyze data through a set of different modalities and conditions. This is also true in scalp electroencephalography (EEG), which is usually carried out at various locations (electrodes), under different conditions, or with a set of subjects. EEG data are also often represented by their time-varying spectral properties using the Fourier or wavelet transformation of raw EEG records. This multimodal nature of EEG data

Zuzana Rošťáková and Roman Rosipal contributed equally to this work.

✉ Zuzana Rošťáková
zuzana.rostakova@savba.sk

Roman Rosipal
roman.rosipal@savba.sk

¹ Institute of Measurement Science, Slovak Academy of Sciences, Dúbravská cesta 9, Bratislava 84104, Slovakia

² Pacific Development and Technology, LLC, 408 Hill Street, Capitola, CA 95010, USA

follows the structure of a multiway array or a tensor, where each modality spans one axis (a mode in tensor terminology). Tensor data structure often occurs in psychometrics, chemometrics, and other research domains [2]. While the tensor represents an appropriate data structure in these fields, a direct interpretation of tensor data is often more complicated. Low-rank representation and latent component identification play an essential role in tensor data analysis.

Tensor decomposition methods have been successfully applied to EEG data, thus leading to new insights and a better understanding of their latent structure and generation sources [3–6]. Such findings are consistent with our over ten years of experience in developing and applying the tensor decomposition methods to different EEG analysis problems [7–10]. The most commonly used approach is parallel factor analysis (PARAFAC) [11, 12]. PARAFAC decomposes a tensor into a set of more accessible and interpretable matrices with the same number of latent components in each mode.

Unfortunately, not all matrix decomposition properties are inherited in tensor decomposition approaches. For example, the number of latent components in PCA is often selected using the explained proportion of variance. In tensor decomposition methods, the number of components K in each mode is an important input parameter that must be determined often in advance. If we choose a K value that is too small, then some latent components will not be recovered. On the other hand, if we choose a K value that is too large, then an unnecessarily complex model will be developed with some components that occur only by chance or that only represent a random part of the data (noise). Moreover, latent sources of variability would be modeled by many correlated components. Furthermore, a PCA model with K components is inherited in a model with $K + 1$ components, although this is not true for the PARAFAC model nor any other tensor decomposition method. These differences make component number selection even more challenging [2].

Many methods and heuristics for choosing an appropriate number of components in tensor decomposition have been proposed in the literature. However, none of them has become a state-of-the-art method. The reason may be that the methods follow different assumptions and computational complexity or were proposed for a specific data type.

The method's performance is usually compared and validated on simulated data with a simplified structure [13–18], but which is not consistent with the real data character [13], or simple real data with a priori known number of components [13, 15–17, 19]. However, we are not aware of any comparative study considering neurophysiological data like the human EEG signal.

Our study analyzes the performance and applicability of twelve component number selection methods to fill this gap. We focus on the domain of PARAFAC decomposition of EEG signal. We aim answering the following questions: Which methods are appropriate, and which are not for the PARAFAC latent component number selection in EEG signal? What is the methods' sensitivity to different types of noise or the method assumption violation?

For this purpose, we simulated data with known and well-controlled properties closely mirroring the real EEG signal character. Finally, following our previous experience and practice, we also include a new approach that we have proposed for selecting the number of latent components in real EEG signal tasks [9]. The method is based on the cumulative clustering of latent components from several tensor decomposition models, and we denote it as *tripleC*.

The article is organized as follows: Sect. 1.1 brings an overview of the related comparative studies, and the problem statement is summarized in Sect. 1.2. Section 2 focuses on the PARAFAC model and component number selection methods used in the study. Nine types of simulated data described in Sect. 3 are then used for the methods' performance comparison in Sect. 4. The advantages and disadvantages of the methods are discussed, and the conclusions are stated in Sect. 5.

1.1 Related studies

Many methods and heuristics for choosing an appropriate number of components in tensor decomposition have been proposed in the literature. As a by-product, they also include a short comparative study highlighting the advantages of their method over competing approaches on simulated data with a known number of latent components. The comparison is based either on a small set of approaches with similar character [13, 16, 17, 20] or on a rich collection of different methods [14, 15, 19, 21].

In these studies, component matrices of a tensor are generated by considering two data types i) the elements of component matrices are generated as independent and identically distributed (iid) random samples from the standard normal distribution $\mathcal{N}(0, 1)$ [14, 15], or ii) component matrices are generated as random matrices with orthonormal columns [16–18]. In both cases, the simulated tensor follows a trilinear structure. The noise terms are generated as iid samples from the normal distribution $\mathcal{N}(0, \sigma^2)$.

The orthogonality assumption simplifies computational issues, and many component number selection methods are directly or indirectly compatible with this assumption. Moreover, component orthogonality was observed to

improve solution stability, such as in psychometrics [22]. However, the premise of orthogonality is often hard to accept and interpret when dealing with real data in chemometrics or neurophysiology domains. The elements of the data tensor are often nonnegative, and also, all or selected components are assumed to be nonnegative [2, 8] or unimodal [8, 23].

Moreover, Bro and Kiers [13] pointed out that data simulated in this way do not necessarily follow the properties of real data, and they observed different behavior of their method when applied to artificial and real data. They stated that “...*These results strongly indicate that none of the real data have characteristics close to the simulated data and that results obtained on data simulated in this way cannot be taken to be indicative for PARAFAC results on real data.*” They stress the fact that real data never follow an exact trilinear structure and include minor deviations [13].

Any article dealing with the component number selection focuses on more complex simulations trying to mimic the real data character. They focus on real chemometric [13, 15, 19], music [16] or social data [17] with the number of components known a priori or from the previous analysis. However, the EEG signal is not considered. Moreover, the proper latent structure and the correct number of components are always questionable in this case.

The comprehensive overview of the EEG signal tensor decomposition of Cong et al. [6] describes the component number selection problem only marginally by mentioning the difference in the method’s fit [18] and an ICA-based approach. The core consistency diagnostics [13], proportion of residual variance or the Bayesian information criterion are considered in neurophysiologically oriented studies [3, 4, 24, 25], or the number of latent components is set manually without detailed explanation [5]. Nevertheless, studies discussing the appropriateness of the selected approaches for EEG data are missing.

1.2 Problem statement

In this study, we aim to clarify the benefits and limits of a set of component number selection methods when dealing with nonnegative EEG data in the time-space-frequency domain where the orthogonality assumption is not met. To reach this objective, we simulated data that closely mimic the character of time-varying human scalp EEGs [10]. Of course, simulated data will never precisely follow the complex structure of real data. Nevertheless, we used a realistic head model and cortical source generation to simulate the real EEG data properties as closely as possible. We also consider data structure variants similar to that in [13, Section 4], with the aim of highlighting potential pitfalls in the considered methods when a systematic

deviation from the trilinear structure is present. This process allows us to compare and highlight the limits of the existing and often used methods for determining the number of components.

2 Methods

The section begins with the basic tensor notation and terminology. Then, a brief concept behind the parallel factor analysis (PARAFAC) [11, 12] is given. Finally, five sets of existing component number selection methods and a new approach are described.

2.1 Notation

The basic notation follows [1]. An underlined bold uppercase letter $\underline{\mathbf{X}} \in \mathbb{R}^{I_1 \times I_2 \times \dots \times I_N}$, an uppercase letter $X \in \mathbb{R}^{J_1 \times J_2}$, a lowercase bold letter $\mathbf{x} \in \mathbb{R}^L$ and a lowercase letter $x \in \mathbb{R}$ stand for an N -way tensor, matrix, vector and scalar, respectively. The normal (Gaussian) and uniform probability distributions are denoted by \mathcal{N} and \mathcal{U} .

The higher-order Frobenius norm of a tensor $\underline{\mathbf{X}} \in \mathbb{R}^{I_1 \times I_2 \times \dots \times I_N}$ [1, Section 1.4.6] is defined as the sum of its squared elements

$$\|\underline{\mathbf{X}}\|_{Fro} = \sqrt{\sum_{i_1=1}^{I_1} \sum_{i_2=1}^{I_2} \dots \sum_{i_N=1}^{I_N} x_{i_1 i_2 \dots i_N}^2}.$$

The ‘hat’ symbol ($\hat{\cdot}$) above a variable represents the corresponding estimate. Finally, we use the formula $x \gg y$ if an x is much larger than y .

2.2 Parallel factor analysis

PARAFAC decomposes an N -way tensor $\underline{\mathbf{X}} \in \mathbb{R}^{I_1 \times I_2 \times \dots \times I_N}$ into N matrices $A^{(n)} = (\mathbf{a}_1^{(n)}, \mathbf{a}_2^{(n)}, \dots, \mathbf{a}_K^{(n)}) \in \mathbb{R}^{I_n \times K}$, where $\mathbf{a}_i^{(n)} \in \mathbb{R}^{I_n}$ denotes the i^{th} column of $A^{(n)}$, $n = 1, \dots, N$, and K is a common number of matrix columns, that is, the number of latent components. The model follows the formula

$$\begin{aligned} \underline{\mathbf{X}} &= \underline{\mathbf{\Lambda}} \times_1 A^{(1)} \times_2 \dots \times_N A^{(N)} + \underline{\mathbf{E}}, \\ x_{i_1 i_2 \dots i_N} &= \sum_{k=1}^K \lambda_k a_{i_1 k}^{(1)} a_{i_2 k}^{(2)} \dots a_{i_N k}^{(N)} + e_{i_1 i_2 \dots i_N}, \\ i_j &= 1, \dots, I_j; \quad j = 1, \dots, N, \end{aligned} \tag{1}$$

where $\times_j, j = 1, \dots, N$ denotes the tensor-matrix product in the j^{th} mode [1], $\underline{\mathbf{\Lambda}} \in \mathbb{R}^{K \times \dots \times K}$ is an N -way superdiagonal tensor with nonzero elements $\lambda_1, \dots, \lambda_K$ only on its main diagonal and the tensor $\underline{\mathbf{E}} \in \mathbb{R}^{I_1 \times \dots \times I_N}$ represents an error

term. To avoid multiplication indeterminacies, the component matrices $A^{(n)}$, $n = 1, \dots, N$ in the PARAFAC model (1) are assumed to have normalized columns [1].

A k^{th} latent component F_k is characterized by the k^{th} column of each component matrix, e.g., $\mathbf{a}_k^{(1)}, \mathbf{a}_k^{(2)}, \dots, \mathbf{a}_k^{(N)}$. In the following text, $\mathbf{a}_k^{(n)}$, $n = 1, \dots, N$ will represent the n^{th} mode of the k^{th} component.

Under mild conditions, the PARAFAC solution was proven to be unique up to a permutation of components' order [26]. Several methods for component number selection rely on this PARAFAC property.

2.3 Component number selection methods

This study divides the component number selection methods into five sets according to their character and assumptions. The number of latent components selected by a given method is denoted as K^* . K_{true} represents the correct number of components and K_{max} denotes the maximal allowed number of components.

i) Visual inspection methods The first set includes the proportion of variance explained (*VarExpl*) [2], the core consistency diagnostics (*CCD*) [13] and the core consistency diagnostics aided by reconstruction error (*CCDaRE*) [20] which is a combination of the previous two. A given measure is computed for PARAFAC models with $K = 2, \dots, K_{\text{max}}$ components and the values are plotted against the number of components. A point preceding a rapid change in the curve profile is visually selected and assigned as the optimal number of components (Fig. 1a).

ii) Methods based on PARAFAC component similarity The nonredundant model order selection (*NORMO*) [19] method examines the similarity between estimated

components of the PARAFAC models with different numbers of extracted components. *NORMO* searches for the largest K^* for which the PARAFAC model extracts a set of nonredundant components only, although in a model with $K^* + 1$ components at least one redundancy occurs. Two components F_i and F_j are considered to be redundant if the average absolute correlation coefficient ρ between their modes

$$R(F_i, F_j) = \frac{1}{N} \sum_{n=1}^N \left| \rho \left(\mathbf{a}_i^{(n)}, \mathbf{a}_j^{(n)} \right) \right|$$

is above a user-defined threshold. In [19], the authors empirically set the threshold to 0.7 with the aim of detecting highly correlated components in at least $N - 1$ modes.

Two *NORMO* versions were proposed: exhaustive (*NORMO_E*) and binary (*NORMO_B*). *NORMO_E* takes into account all PARAFAC models with $K = 2, \dots, K_{\text{max}}$ components. *NORMO_B* iteratively halves the set of all possible K values until only one value $K = K^*$ remains [19].

In our previous studies, we used the approach we denote here as *tripleC* [9, 27]. The method operates on the similar principle of investigating similarities of extracted modes from the PARAFAC models of different $K = 2, \dots, K_{\text{max}}$.

TripleC first merges components from all considered PARAFAC models into one set and then applies a cluster analysis with the aim of detecting homogeneous clusters of similar components. The similarity across different modes can be treated and weighted differently following their dimension and property. Although PARAFAC with K components is not completely inherited in the model with $K + 1$ components, we assume that the most specific components occur frequently and form the dominant clusters. A cluster is considered “dominant” if the ratio R_{tripleC} of its cardinality and the number of considered PARAFAC models ($K_{\text{max}} - 1$) is above 50%. This threshold initially appears to be low; however, we must consider that in PARAFAC with $K < K_{\text{true}}$ components, not all target components are present. Moreover, $R_{\text{tripleC}} > 1$ is also possible. When $K \gg K_{\text{true}}$, PARAFAC models include many redundant components; therefore, a target component may occur in the model more than once. Finally, the number of dominant clusters is considered to be the optimal K^* .

Different clustering methods have been proposed in the literature. However, methods that require determining the number of clusters in advance are not appropriate for *tripleC*. Our practical experience shows that the best results are often obtained with density-based clustering (DBscan) [28]. DBscan automatically finds the best suitable number of clusters. Moreover, components showing a high level of

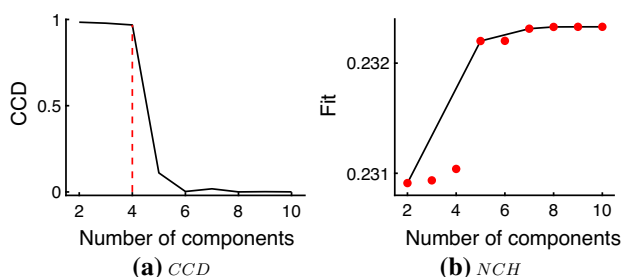


Fig. 1 **a** Example of the core consistency diagnostics (*CCD*) behavior (solid black line) for a randomly chosen trial from the simulated D_0 dataset described in Sect. 3. A rapid drop in the *CCD* profile is observed following the selection of four components (dashed red line). **b** Fit (red dots) in PARAFAC models with the varying number of latent components for a randomly chosen trial from the $DBBA_{\text{low}}$ dataset described in Sect. 3. Numerical convex hull (*NCH*) approach counts only on PARAFAC models whose fit (red dots) lays on the fit's convex hull boundary (black line)

dissimilarity with the other components can be identified as noise and ignored. DBscan requires setting the minimum number of neighbors parameter, which we set to two, and the diameter of the epsilon neighborhood, which we fixed to 0.5 [28].

iii) Methods based on the PARAFAC model fit A fit of the PARAFAC model with K components is defined as

$$fit(K) = \|\underline{\mathbf{X}}\|_{Fro}^2 - \|\underline{\mathbf{X}} - \hat{\underline{\mathbf{A}}} \times_1 \hat{\mathbf{A}}^{(1)} \times_2 \dots \times_N \hat{\mathbf{A}}^{(N)}\|_{Fro}^2, \\ \hat{\mathbf{A}}^{(n)} \in \mathbb{R}^{I_n \times K}, \quad n = 1, \dots, N.$$

The difference in fit (*DIFFIT*) [18] searches for the maximal relative change in fit between PARAFAC models with a consecutive number of components

$$DIFFIT(K) = \frac{fit(K) - fit(K - 1)}{fit(K + 1) - fit(K)}, \\ fit(1) = 0, \\ K = 2, \dots, K_{max} - 1.$$

However, computing the fit of all PARAFAC models with $K = 2, \dots, K_{max}$ components is time-consuming, especially when K_{max} is large. Kiers and der Kinderen [17] obtained results comparable to *DIFFIT* but with significantly lower computational time using the approximate fit (*FastDIFFIT*). The numerical convex hull (*NCH*) [16] also operates on the approximate fit, although only models with the approximate fit lying on the convex hull boundary are taken into account (Fig. 1b).

iv) Methods based on eigenvalue analysis The fourth set of methods works with the matricized (unfolded) versions of a tensor. A tensor is transformed into a matrix by stacking its slices rowwise or columnwise [1].

The minimal description length approach (*MDL*) [14] minimizes a penalized negative log-likelihood function by using eigenvalues of $2^{N-1} - 1$ matrix versions of the N -way tensor. However, *MDL* was shown to be sensitive to the presence of strong noise [21]. Therefore, the sparse core method (*SCORE*) and the modified eigenvalue estimation for Tucker rank determination (*MEET*) [21], as methods using modified eigenvalue estimates, were proposed to improve *MDL* stability and robustness.

Nevertheless, K^* selected by any of the three methods was always equal to the minimal size of the tensor in all datasets considered in this study. These problems were mainly associated with numerical issues due to the close-to-zero eigenvalues. For *MDL* and *MEET*, we observed better results when considering only the first few largest eigenvalues so as their cumulative variance explained exceeds a user-defined threshold α . Empirically, we selected $\alpha_{MDL} = 0.9$ for *MDL* and $\alpha_{MEET} = 0.78$ for *MEET*.

For *SCORE*, it is important to appropriately set the ρ_{SCORE} parameter [21, Section 5]. In this case, the ρ_{SCORE} values varied between 10^{-4} and 10^{-3} according to the level of noise in the data.

v) Methods based on Bayesian statistics Automatic relevance determination (*ARD*) [15] assumes that the component matrix elements follow either normal or Laplacian distributions, thus leading to the ridge (*ARD_R*) or sparse (*ARD_S*) version of *ARD*. When latent components are assumed to be nonnegative, the prior distribution becomes rectified normal in *ARD_R* and exponential in *ARD_S*.

The algorithm starts by fitting the PARAFAC model with the largest allowed number of components K_{max} . Each iteration step consists of updating components followed by pruning out the components with their Euclidean norm under a given small threshold β . Consequently, the number of components iteratively decreases until the algorithm converges.

However, after applying the *ARD* method to our data in Sect. 3, the resulting number of components was always equal to K_{max} , which was caused by too small default β value [15]. By varying this parameter, we observed that the optimal results were obtained by applying different threshold values for each data type. In other words, it was possible to set the optimal β only based on a priori knowledge about the valid data structure. Different threshold values led to different K^* choices.

To mitigate this problem, we proposed the following modified criterion for pruning out the components with a small Euclidean norm. In the i^{th} iteration step, we fit PARAFAC with K_i components. These components are ordered according to their Euclidean norms in ascending order. Let us denote these ordered weights as $\gamma_1 \leq \gamma_2 \leq \dots \leq \gamma_{K_i}$. Then, the f^{th} component is pruned out if

$$1 - \frac{\gamma_f}{\sum_{l=1}^{K_i} \gamma_l} > \alpha_{ARD},$$

where α_{ARD} is a user-defined threshold. In this study, we empirically selected $\alpha_{ARD} = 0.95$. This criterion is a heuristic, although it also shows more general applicability than the original criterion. Moreover, a similar rule was also used in [29].

Mørup and Hansen [15] recommended to avoid component removal in the first few iterations due to poor model estimates. For most data types considered in this study, we rejected component removal in the first 25 iterations. For one data type, the number of iterations was reduced to 10 due to the rapid convergence of the algorithm. Details are provided in Sect. 4.5.

General setting across methods The *VarExpl*, *CCD*, *NORMO*, *tripleC*, *DIFFIT*, and *ARD* methods require the identification of the maximal number of components K_{max}

up to which the corresponding PARAFAC models should be computed. The remaining methods work with all component number possibilities up to the size of the tensor (I_1, I_2, \dots, I_N) . Since it would be time-consuming to fit all PARAFAC models with $K = 2, \dots, \min(I_1, I_2, \dots, I_N)$ and the correct number of components in our simulated data is much lower than $\min(I_1, I_2, \dots, I_N)$ (see Sect. 3), we decided to restrict the maximal allowed number of components K_{max} to 10. Consequently, if a method selected $K^* > 10$, we set it to 10.

Whenever possible, a priori information about the non-negativity data structure was incorporated into the method. Unfortunately, *FastDIFFIT*, *NCH* and the methods based on eigenvalue analysis (*MDL*, *MEET*, and *SCORE*) do not allow for the application of a priori knowledge or assumptions about the data structure.

3 Data

We considered three types of simulated data with well-controlled properties. The datasets generated and analyzed during the current study are available from the corresponding author on reasonable request.

Type I data: Simulated EEG data The EEG signal simulation follows the methods of Cohen [30]. A human cortex is represented by 2004 dipoles placed in gray matter. We generated one minute of broadband brain activity (BBA) for each dipole, with a sampling rate of 256 Hz. In [30], BBA was simulated as a smoothed random signal generated from the standard normal distribution. However, such a signal does not mimic the well-known $1/f$ property of the background EEG in the frequency domain [31]. Therefore, we prefer using a realization of the fractional Brownian motion with the Hurst exponent $H = 0.6$ (Fig. 2, bottom).

Then, seven dipoles were selected to represent sources of four oscillatory rhythms: (1) a θ rhythm (5 Hz, Fig. 2, blue) located in the frontal cortical region, (2) a μ rhythm (8 Hz, Fig. 2, green) located in the somatosensory cortex, (3) a visual α rhythm (9 Hz, Fig. 2, yellow) located in the occipital cortical region, and (4) a β rhythm (14 Hz, Fig. 2, red) located in the somatomotor cortex. The μ , α and β activity sources were placed symmetrically in both the left and right hemispheres. Narrow-band oscillatory rhythms were generated as a sinusoidal signal with a random modulation of frequency and amplitude at each time point. Random modulation was performed in the frequency domain by applying the convolution of the Gaussian kernel and randomly generated noise with a normal distribution. The peak frequency and full width at half maximum of this filter were set to 15 Hz. One minute of the continuous signal was generated for each oscillation frequency. The

time activation of each rhythm was controlled by applying a Hann window of varying length between five and ten seconds. The time activation of each of the four oscillatory rhythms was generated as nonoverlapping in time (Fig. 2, right).

Finally, a forward model was applied to map the source cortical signal of 2004 dipoles to the human skull. The model was computed using the Brainstorm toolbox [32] in MATLAB [33]. This results in simulated EEG time series as measured by 64 scalp electrodes arranged according to the international 10–20 system.

According to the ratio between the amplitude of the target oscillations and BBA, we distinguish clear data with the absence of BBA (D_0 , ratio = 0) and data with low ($DBBA_{low}$, ratio = 0.2) and high ($DBBA_{high}$, ratio = 0.8) levels of BBA. For each data type, we generated 50 trials.

Type II data: Simulated EEG data with four oscillations and Gaussian noise In the second step, we added normally distributed (Gaussian) noise to the D_0 data. The variance of the noise was chosen such that the signal-to-noise ratio (SNR) was approximately equal to the SNR of $DBBA_{low}$ and $DBBA_{high}$ data. We generated and used 50 trials of each DG_{low} and DG_{high} dataset.

Type III data: Simulated data with a deviation from the trilinear structure The PARAFAC model with four components was applied to a randomly selected D_0 dataset (Fig. 3). Then, new data were generated by back-multiplying the estimated component matrices $\hat{A}^{(1)}$, $\hat{A}^{(2)}$, and $\hat{A}^{(3)}$ and by adding two types of “variation”

$$\begin{aligned} \underline{X} &= \underline{X}_0 + c_y \underline{Y} + c_e \underline{E} \\ \underline{X}_0 &= \underline{I}_3 \times_1 \hat{A}^{(1)} \times_2 \hat{A}^{(2)} \times_3 \hat{A}^{(3)}. \end{aligned} \quad (2)$$

The tensor $\underline{I}_3 \in \mathbf{R}^{4 \times 4 \times 4}$ represents a superdiagonal three-way tensor, which includes ones on its main diagonal and zeros elsewhere. The tensor \underline{X}_0 characterizes the part of data that follows a pure trilinear structure. A minor deviation from the trilinear structure is represented by the \underline{Y} term (2). It was generated in the following way

$$\begin{aligned} \underline{Y} &= \underline{G} \times_1 \hat{A}^{(1)} \times_2 \hat{A}^{(2)} \times_3 \hat{A}^{(3)} \\ \underline{G} &\in \mathbb{R}^{4 \times 4 \times 4}, \quad g_{ijk} \sim \mathcal{U}(0, 1). \end{aligned} \quad (3)$$

The elements of the noise tensor \underline{E} were generated as independent and identically distributed (iid) random samples from the normal distribution $\mathcal{N}(0, 1)$

$$\underline{E} \in \mathbb{R}^{I_1 \times I_2 \times I_3}, \quad e_{ijk} \sim \mathcal{N}(0, 1).$$

Constants c_y and c_e influence the proportion of deviation from the trilinear structure. We considered four cases:

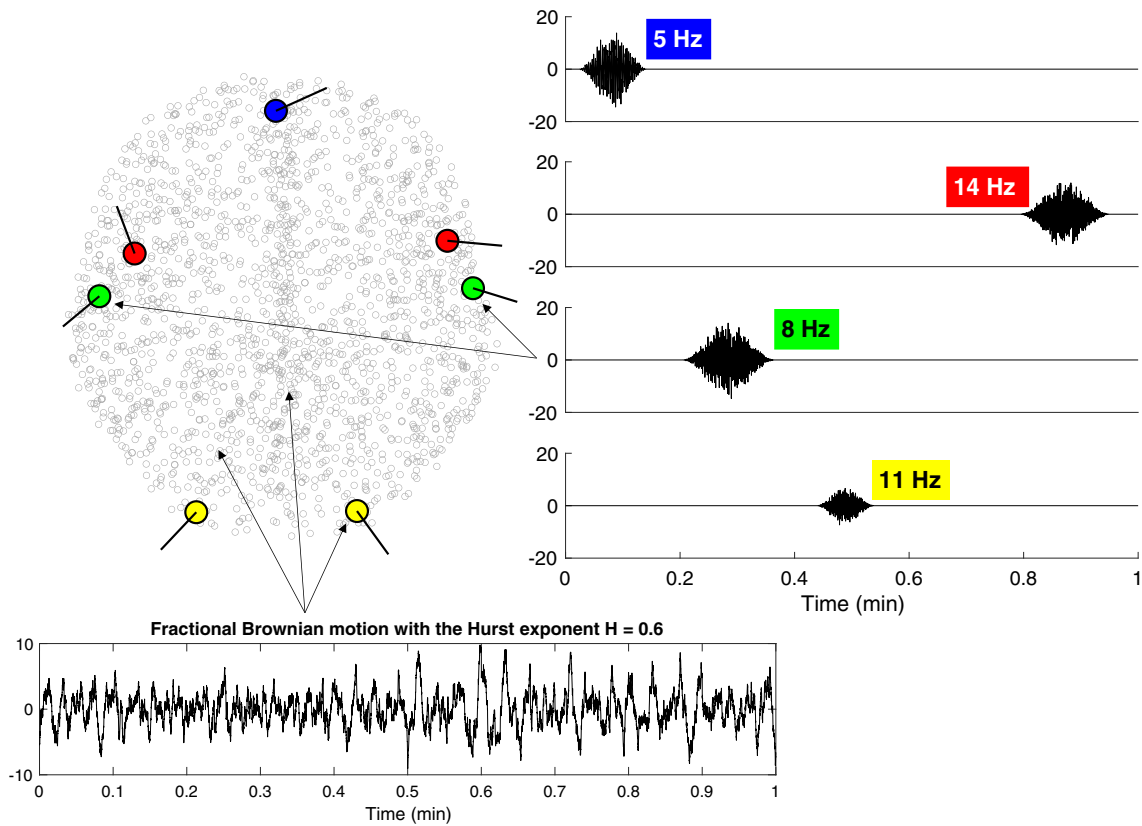
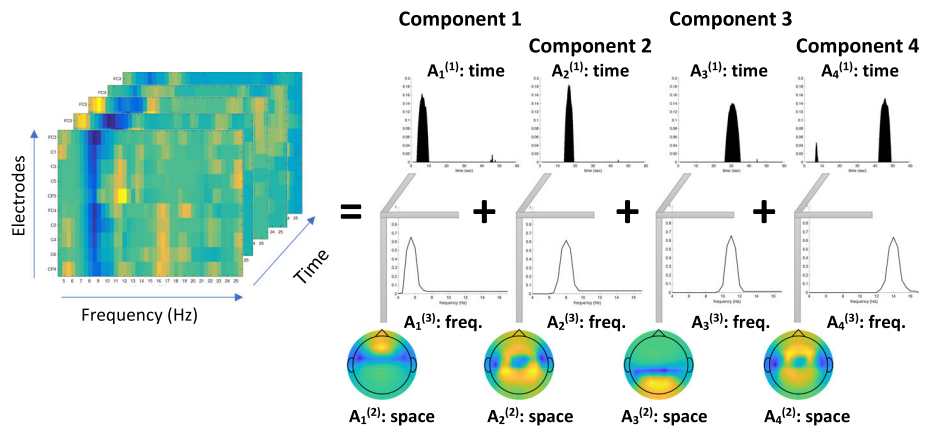


Fig. 2 Human cortex represented by 2004 dipoles; top view (figure on the left). One minute of broadband brain activity was generated for each dipole to follow the fractional Brownian motion (bottom). Seven dipoles were selected as sources of oscillatory activity at 5 Hz (blue),

8 Hz (green), 11 Hz (yellow) and 14 Hz (red). The time activation of each oscillatory rhythm (right) was simulated as nonoverlapping with each other

Fig. 3 Graphical scheme of the parallel factor analysis with four components applied to a randomly chosen realization from the D_0 dataset (see text)



$$\begin{aligned}
 DTri_{11} : \quad c_y &= 0.045 \frac{\|X_0\|_{Fro}^2}{\|Y\|_{Fro}^2} & c_e &= 0.005 \frac{\|X_0\|_{Fro}^2}{\|E\|_{Fro}^2} \\
 DTri_{12} : \quad c_y &= 0.005 \frac{\|X_0\|_{Fro}^2}{\|Y\|_{Fro}^2} & c_e &= 0.045 \frac{\|X_0\|_{Fro}^2}{\|E\|_{Fro}^2} \\
 DTri_{21} : \quad c_y &= 0.9 \frac{\|X_0\|_{Fro}^2}{\|Y\|_{Fro}^2} & c_e &= 0.1 \frac{\|X_0\|_{Fro}^2}{\|E\|_{Fro}^2} \\
 DTri_{22} : \quad c_y &= 0.1 \frac{\|X_0\|_{Fro}^2}{\|Y\|_{Fro}^2} & c_e &= 0.9 \frac{\|X_0\|_{Fro}^2}{\|E\|_{Fro}^2}
 \end{aligned}$$

The data possess either 5% ($DTri_{11}, DTri_{12}$) or 100% ($DTri_{21}, DTri_{22}$) disruption from a pure trilinear structure. In all cases, the ratio between the deviation from the trilinear structure (Eq. 3), and Gaussian noise is either 9:1 ($DTri_{11}$ and $DTri_{21}$ data) or 1:9 ($DTri_{12}$ and $DTri_{22}$ data). Similar data were simulated by Bro and Kiers [13].

Data preprocessing The Type III data are already in tensor form, and no preprocessing step is needed.

However, the simulated Type I and Type II EEG data form a matrix of size $T \times 64$, where T is the number of generated time points and 64 represents the number of electrodes. In the first step, the simulated signal from each electrode was divided into 2-second long time windows with 95% (1.9 sec) overlaps. Then, for each time window, the oscillatory part of the signal amplitude spectrum was extracted by the irregular resampling auto-spectral analysis (IRASA) method [34]. An oscillatory amplitude spectrum in the range of 4 to 25 Hz was used. Note that a similar procedure led to good results when applied to real EEG signals in our previous study [9].

4 Results

The section is divided into five subsections corresponding to the five sets of component number selection methods.

4.1 Visual inspection methods

Manual selection of K^* by using the *VarExpl* plots led to systematic overestimation of K_{true} (Fig. 5a). We were not able to select the true number of four components in the $D_{Tri_{11}}$ and $D_{Tri_{12}}$ datasets, which represent data with only 5% variation from the trilinear structure. For the simulated EEG data D_0 and DG_{low} , *VarExpl* selected $K^* = 4$ in a slightly more than half of the trials. However, the method fails when dealing with a higher level of Gaussian noise (DG_{high}) or the presence of BBA ($DBBA_{low}$, $DBBA_{high}$). Moreover, *VarExpl* increased approximately constantly with increasing K , and the visual selection of K^* in the *VarExpl* plots was challenging in these cases (Fig. 4, left).

The *CCD* method performed well on the $D_{Tri_{11}}$ and D_0 datasets (Fig. 5b), and four components were selected as optimal in the majority of trials. However, for the other datasets, the selected K^* varied in the range between two and seven. Similar to *VarExpl*, the method faced problems for simulated EEG data and failed in the case of the most complex $DBBA_{high}$ dataset. The main problem appears again to be the absence of a rapid change in the *CCD*

profile (Fig. 4, right), leading to a high level of subjectivity in the K^* choice.

CCDaRE did not overcome the *CCD* outcomes (Fig. 5c), and we assumed that this was due to the poor performance of *VarExpl*, which failed to improve the *CCD* performance.

4.2 Methods based on PARAFAC component similarity

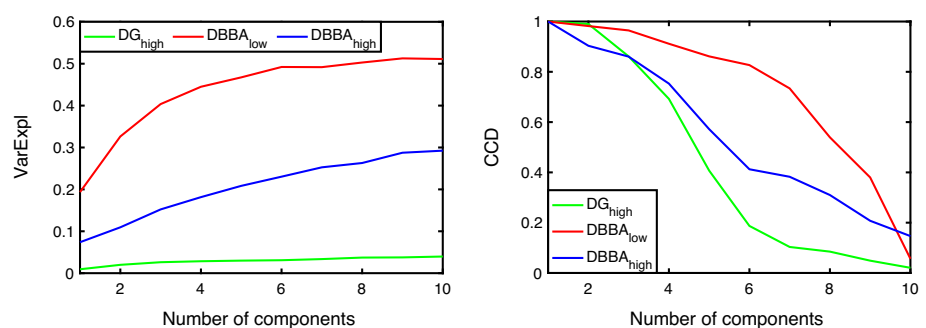
The computational time of the $NORMO_E$ method was longer, but the method produced better results than $NORMO_B$. Therefore, only the results of $NORMO_E$ are presented in this study (Fig. 5d).

$NORMO_E$ selected $K^* = 4$ in the majority of $D_{Tri_{11}}$ trials. For the other datasets, $K^* = 4$ was observed in less than 44% of trials. For DG_{high} and $DBBA_{high}$, the method was not able to determine a K^* value lower than the maximal allowed number of components. We observed that the major problem was the numerically weak correlations between the estimated components due to Gaussian noise or BBA added. However, a visual inspection of the estimated components recovered a high similarity between their characteristics from a physiological point of view.

As depicted in Fig. 5e, *tripleC* successfully selected $K^* = 4$ in the majority of datasets with a small variation from the trilinear structure. This is also true in the case of simulated EEG data that included either four oscillations (D_0) only or also after adding Gaussian noise with low variance (DG_{low}).

The results suggest that *tripleC* slightly underestimates the component number when a higher level of Gaussian noise is present ($D_{Tri_{22}}$, DG_{high}). For datasets with BBA, the selected component number varied between four and five. *TripleC* is a heuristic, but it outperformed $NORMO$ and other visual inspection methods. This cumulative component clustering approach was successfully used in our previous studies that used real EEG data; therefore, good performance on simulated data was expected.

Fig. 4 Example of the *VarExpl* (left) and *CCD* (right) profiles computed for randomly selected trials of the DG_{high} , $DBBA_{low}$, and $DBBA_{high}$ datasets described in details in Sect. 3. The datasets generated and analyzed during the current study are available from the corresponding author on reasonable request



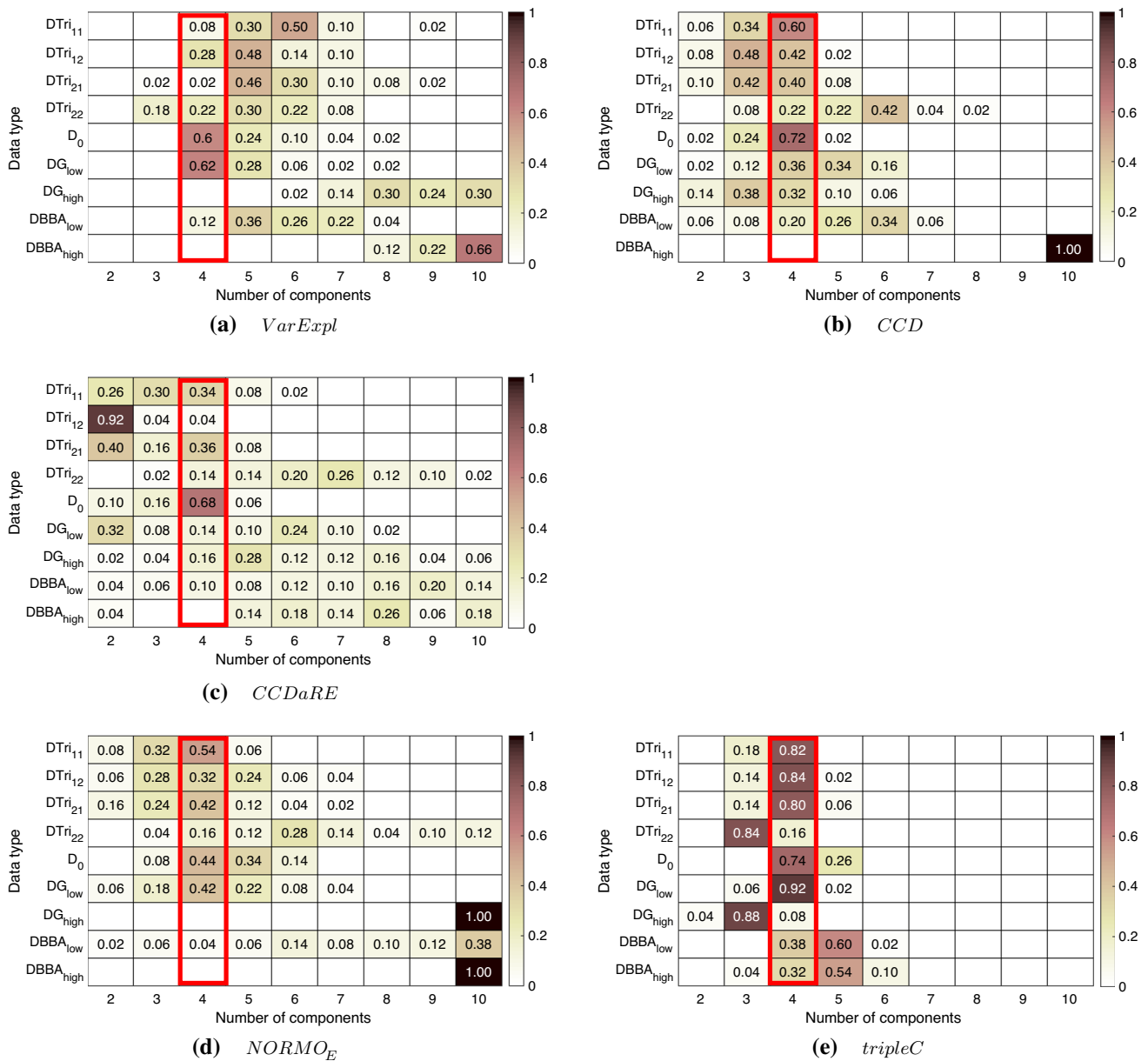


Fig. 5 Proportion of selected number of components ($K = 2, \dots, 10$) in 50 trials using nine datasets obtained by the manual visual inspection of the variance explained (*VarExpl*) and core consistency diagnostics (*CCD*) plots, or automatically by the core consistency diagnostics aided by reconstruction error (*CCDaRE*), the exhaustive

non-redundant model order selection (*NORMOE*) and cumulative component clustering (*tripleC*) methods. Only nonzero values are depicted. The red rectangle depicts the true number of four components

4.3 Methods based on the PARAFAC model fit

The difference in fit (*DIFFIT*) performed poorly for all considered types of data (Fig. 6a). The selected K^* varied between three and nine. However, since the PARAFAC model's fit and *VarExpl* are highly related, the observed poor performance of *VarExpl* predicts inferior results for *DIFFIT*.

The *FastDIFFIT* and *NCH* methods both use the approximate fit and performed well on the DTr_{i11}, DTr_{i12}

and DTr_{i21} datasets, where they outperformed *tripleC* (Fig. 6b and 6c). Similar to *tripleC*, their performance for DTr_{i22} deteriorated due to the presence of a higher proportion of Gaussian noise. However, compared with *tripleC*, the performance of *FastDIFFIT* and *NCH* declined when considering simulated EEG data, regardless of the presence of BBA or Gaussian noise.

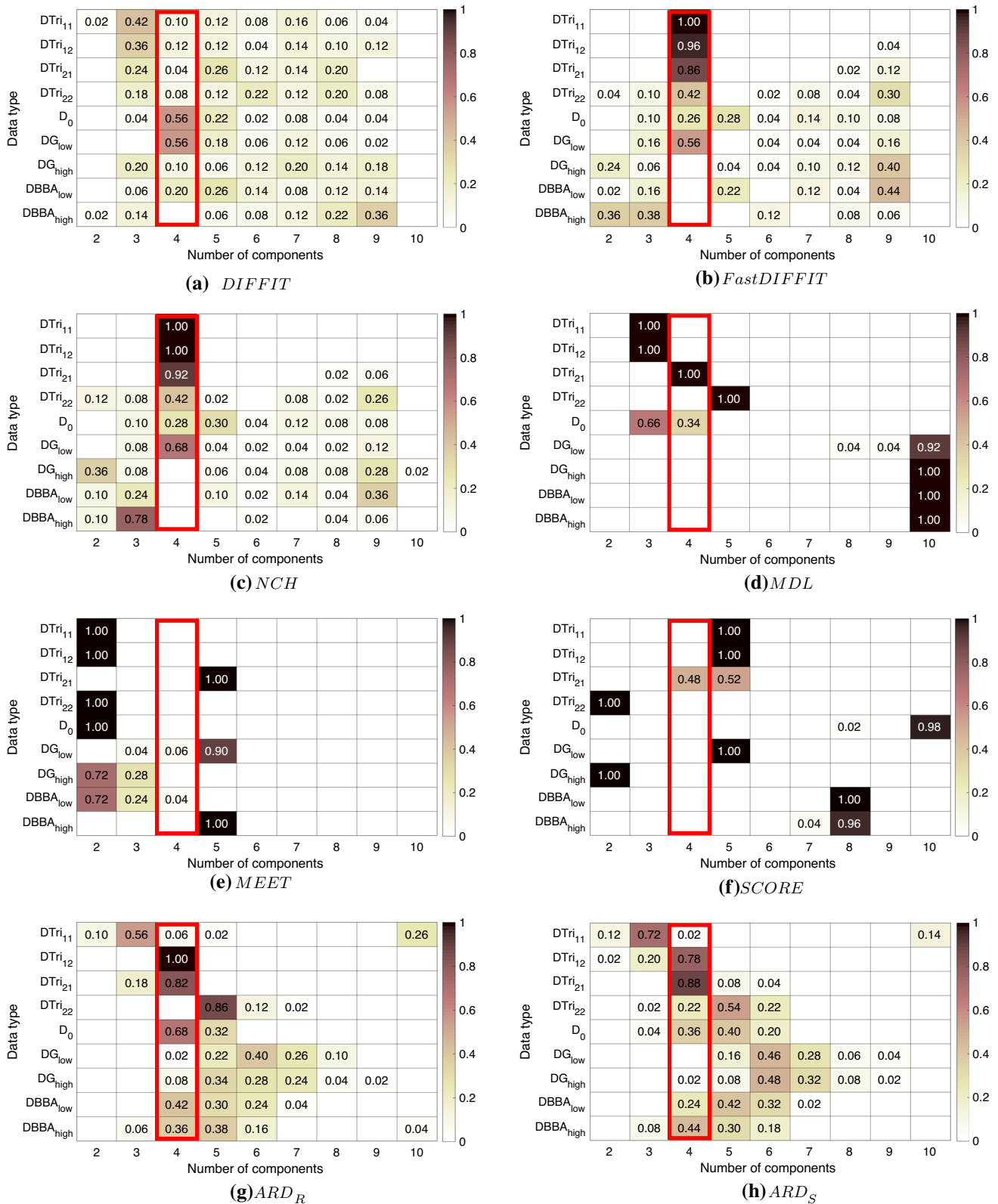


Fig. 6 Proportion of selected number of components ($K = 2, \dots, 10$) in 50 trials using nine datasets obtained by the difference in fit (*DIFFIT*) and its fast version (*FastDIFFIT*), numerical convex hull (*NCH*), minimal description length (*MDL*), modified eigenvalue estimation for Tucker rank determination (*MEET*), sparse core

(*SCORE*) method and ridge and sparse version of the automatic relevance determination (*ARD_R*, *ARD_S*) methods. Only nonzero values are depicted. The red rectangle depicts the true number of four components

4.4 Methods based on eigenvalue analysis

MDL, *MEET* and *SCORE* behaved similarly on each dataset. The methods selected at most two different K^* values among 50 trials (Fig. 6d, e, and f), indicating consistency in their outcome. However, the true $K^* = 4$ was selected only sporadically.

MDL selected K^* close to the true four components for the four datasets with a small deviation from the trilinear structure (Fig. 6d). This finding indicates that *MDL* should also perform well on real nonnegative data with a minor deviation from the trilinear structure or the presence of Gaussian noise. However, problems occurred on simulated EEG data, for which *MDL* failed to reduce the maximal allowed number of components in the presence of BBA or Gaussian noise.

We also tested the *MEET* and *SCORE* algorithms, where numerical correction of eigenvalues was proposed to improve *MDL* behavior [21]. However, although the *SCORE* algorithm produced acceptable results for trilinear data and DG_{low} datasets, for the other datasets, it chose either the lowest or the highest allowed number of components (Fig. 6f). Moreover, *MEET* showed inferior performance when compared to *SCORE* (Fig. 6e).

To improve *MDL*, *MEET* or *SCORE* performance, we carefully tuned the thresholds α_{MDL} and α_{MEET} in *MDL* and *MEET* and ρ_{SCORE} in *SCORE*, but without noticeable improvement.

4.5 Methods based on Bayesian statistics

Two *ARD* versions, ARD_R and ARD_S , produced similar results. We expected that ARD_S would lead to a lower K^* than ARD_R , but we did not observe any significant difference between the K^* selection by ARD_R and ARD_S . We hypothesized that the difference between these two *ARD* versions may be more pronounced in the other tensor decomposition methods, e.g., the Tucker model [35]; however, this is a question for further research.

For $DTri_{11}$ and $DBBA_{high}$ data, ARD_R was unable to reduce the maximal allowed number of components $K_{max} = 10$. In the first case, the algorithm's convergence in the first few iterations avoided pruning out any component. Note that the algorithm did not allow for pruning out any component in the first 25 iterations. We solved the problem by reducing this number to 10. For the $DBBA_{high}$ data, the problem was associated with the presence of BBA with high amplitude, although lowering the threshold α_{ARD} for removing the unnecessary components to 0.9 also solved this issue.

Both *ARD* versions worked well for trilinear data. The selected K^* was close to four, which makes the results

comparable to the *tripleC*, *FastDIFFIT* and *NCH* approaches. When dealing with simulated EEG data, *ARD* outperformed methods based on the approximate fit but not the *tripleC* approach.

5 Conclusion

We compared five different sets of component number selection methods on simulated data with a nontrivial and nonnegative structure. We considered two types of simulated EEG data; data with BBA or Gaussian noise and data with a minor deviation from the trilinear structure and Gaussian noise.

The simulated data results indicate that the visual inspection methods, methods based on eigenvalue analysis and the *NORMO* approach are not appropriate for component number selection in EEG tensor decomposition.

The methods based on eigenvalue analysis produced the worst results from all considered methods. When working with eigenvalues, we indirectly assume that the components are orthogonal or close to orthogonal. However, this condition is not fulfilled in any of the considered datasets. Although all three methods were proven to perform well on other types of data [21], we recommend not using them when PARAFAC is applied to real EEG data represented by nonnegative features. In this case, the orthogonality of the components does not make much sense from an interpretation perspective.

The core consistency diagnostics (*CCD*) was used for component number selection in several EEG tensor decomposition studies [3, 4, 24], but without warranting the method's appropriateness. We showed that *CCD*, together with *VarExpl* and *CCDaRE*, produced inferior results for the most superficial data that presented a minor deviation from the trilinear structure. This result is consistent with our previous study focusing on EEG tensor decomposition in post-stroke patients [9], where *CCD* and *VarExpl* were observed to change approximately linearly with the increasing number of components without a rapid drop allowing us to select an optimal number of components visually. Moreover, the poor performance of *CCDaRE* was somewhat expected due to the inferior results of *CCD* and *VarExpl*. Finally, a disadvantage of these approaches is the need to visually inspect plot profiles, which brings high subjectivity when selecting the final component number.

The core problem of the *NORMO* failure lies in numerically weak correlations between physiologically similar components when noise or BBA is present. Therefore, we expect the inferior performance of *NORMO* also in real data cases, as both noise and BBA are always present in the real EEG signal.

For nonnegative real data describing complex phenomena, such as EEG, we recommend either using the *tripleC* or *ARD* approach. *FastDIFFIT* or *NCH* are also good candidates, although they do not incorporate restrictions to latent components, such as the desired nonnegativity. Therefore, they provide the same results regardless of whether a priori information about the data character is available. On the other hand, *ARD* and *tripleC* can work with any reasonable restriction applied to latent components.

Moreover, *ARD* and *tripleC* showed to be less sensitive to the presence of noise or BBA, leading to only a slight overestimation of the correct number of components. On the other hand, *NCH* and *fastDIFFIT* produced less consistent results in this case.

The disadvantage of *tripleC* is the need to estimate components in a sufficiently high number of PARAFAC models, which increases its computational and time costs. In this sense, *FastDIFFIT* and *NCH* are the fastest methods.

Despite all positive results presented in the study, component number selection in PARAFAC remains a challenging problem, which is particularly true when data follow a nonnegative and complex structure. Because information about the true data structure is usually not known when dealing with real data, the most suitable component number selection method cannot be selected a priori. Therefore, one may still combine strict component number selection with an exploratory approach in which the selected components are visually inspected and their relevance interpreted. *TripleC* is a promising approach in this direction.

Acknowledgements This research was supported by the Scientific Grant Agency of the Ministry of Education, Science, Research and Sport of the Slovak Republic and Slovak Academy of Sciences (VEGA grant 2/0023/22) and by the Slovak Research and Development Agency (Grant No. APVV-16-0202).

Author contributions Both authors contributed to the study conception and design. Data simulation and analysis were performed by Zuzana Rošťáková and Roman Rosipal. The first draft of the manuscript was written by Zuzana Rošťáková and both authors commented on previous versions of the manuscript. Both authors read and approved the final manuscript.

Funding This research was supported by the Scientific Grant Agency of the Ministry of Education, Science, Research and Sport of the Slovak Republic and Slovak Academy of Sciences (VEGA grant 2/0023/22) and by the Slovak Research and Development Agency (grant APVV-16-0202).

Data availability Simulated data and source files can be sent on request from the corresponding author Zuzana Rošťáková.

Code availability The MATLAB scripts for data simulation and the cumulative component clustering method (*tripleC*) can be sent on request from the corresponding author Zuzana Rošťáková.

Declarations

Conflict of interest The authors have no competing interests to declare that are relevant to the content of this article.

Ethical approval Not applicable

Consent to participate Not applicable

Consent for publication Not applicable

References

- Cichocki A, Zdunek R, Phan AH, Amari S (2009) Nonnegative matrix and tensor factorizations: applications to exploratory multi-way data analysis and blind source separation. Wiley, United Kingdom
- Bro R (1997) PARAFAC. Tutorial and applications. Chemom Intell Lab Syst 38(2):149–171. [https://doi.org/10.1016/S0169-7439\(97\)00032-4](https://doi.org/10.1016/S0169-7439(97)00032-4)
- Miwakeichi F, Martínez-Montes E, Valdés-Sosa PA, Nishiyama N, Mizuhara H, Yamaguchi Y (2004) Decomposing EEG data into space-time-frequency components using Parallel Factor Analysis. NeuroImage 22(3):1035–1045. <https://doi.org/10.1016/j.neuroimage.2004.03.039>
- Mørup M, Hansen LK, Herrmann CS, Parnas J, Arnfred SM (2006) Parallel factor analysis as an exploratory tool for wavelet transformed event-related EEG. NeuroImage 29(3):938–947. <https://doi.org/10.1016/j.neuroimage.2005.08.005>
- Jannek D, Roemer F, Weis M, Haardt M, Husar P (2009) Identification of signal components in multi-channel EEG signals via closed-form PARAFAC analysis and appropriate preprocessing. In: Vander Sloten J, Verdonck P, Nyssen M, Haueisen J (eds.) 4th European Conference of the International Federation for Medical and Biological Engineering, vol. 22, pp 1226–1230. Springer, Switzerland. https://doi.org/10.1007/978-3-540-89208-3_293
- Cong F, Lin Q-H, Kuang L-D, Gong X-F, Astikainen P, Ristanieni T (2015) Tensor decomposition of EEG signals: A brief review. J Neurosci Methods 248:59–69. <https://doi.org/10.1016/j.jneumeth.2015.03.018>
- Rosipal R, Trejo LJ, Nunez PL (2009) Application of multi-way EEG decomposition for cognitive workload monitoring. In: Vinzi VE, Tenenhaus M, Guan R (eds.) Proceedings of the 6th International Conference on Partial Least Squares and Related Methods, pp 145–149. Electronic Industrial Press of China, China
- Rosipal R, Porubcová N, Barančok P, Cimrová B, Farkaš I, Trejo LJ (2019) Effects of mirror-box therapy on modulation of sensorimotor EEG oscillatory rhythms: a single-case longitudinal study. J Neurophysiol 121(2):620–633. <https://doi.org/10.1152/jn.00599.2018>
- Rošťáková Z, Rosipal R, Seifpour S, Trejo LJ (2020) A comparison of non-negative Tucker decomposition and parallel factor analysis for identification and measurement of human EEG rhythms. Meas Sci Rev 20(3):126–138. <https://doi.org/10.2478/msr-2020-0015>
- Rosipal R, Rošťáková Z, Trejo LJ (2022) Tensor decomposition of human narrowband oscillatory brain activity in frequency, space and time. Biol Psychol 169:108287. <https://doi.org/10.1016/j.biopsycho.2022.108287>
- Harshman RA (1970) Foundations of the PARAFAC procedure: Models and conditions for an “explanatory” multimodal factor analysis. UCLA Working Papers in Phonetics 16, 1–84
- Carroll JD, Chang J-J (1970) Analysis of individual differences in multidimensional scaling via an N-way generalization of

- “Eckart-Young” decomposition. *Psychometrika* 35(3):283–319. <https://doi.org/10.1007/BF02310791>
13. Bro R, Kiers HAL (2003) A new efficient method for determining the number of components in PARAFAC models. *J Chemom* 17(5):274–286. <https://doi.org/10.1002/cem.801>
 14. Liu K, da Costa JPCL, So HC, Huang L, Ye J (2016) Detection of number of components in CANDECOMP/PARAFAC models via minimum description length. *Digital Signal Process* 51:110–123. <https://doi.org/10.1016/j.dsp.2016.01.003>
 15. Mørup M, Hansen LK (2009) Automatic relevance determination for multi-way models. *J Chemom* 23(7–8):352–363. <https://doi.org/10.1002/cem.1223>
 16. Ceulemans E, Kiers HAL (2006) Selecting among three-mode principal component models of different types and complexities: A numerical convex hull based method. *Br J Math Stat Psychol* 59(1):133–150. <https://doi.org/10.1348/000711005X64817>
 17. Kiers HAL, der Kinderen A (2003) A fast method for choosing the numbers of components in Tucker3 analysis. *Br J Math Stat Psychol* 56(1):119–125. <https://doi.org/10.1348/000711003321645386>
 18. Timmerman ME, Kiers HAL (2000) Three-mode principal components analysis: Choosing the numbers of components and sensitivity to local optima. *Br J Math Stat Psychol* 53(1):1–16. <https://doi.org/10.1348/000711000159132>
 19. Fernandes S, Fanaee-T H, Gama J (2020) NORMO: A new method for estimating the number of components in CP tensor decomposition. *Eng Appl Artif Intell*. <https://doi.org/10.1016/j.engappai.2020.103926>
 20. Liu K, So HC, da Costa JPCL, Huang L (2013) Core consistency diagnostic aided by reconstruction error for accurate enumeration of the number of components in PARAFAC models. In: *IEEE international conference on acoustics, speech and signal processing*, pp 6635–6639. <https://doi.org/10.1109/ICASSP.2013.6638945>
 21. Yokota T, Lee N, Cichocki A (2017) Robust multilinear tensor rank estimation using higher order singular value decomposition and information criteria. *IEEE Trans Signal Process* 65(5):1196–1206. <https://doi.org/10.1109/TSP.2016.2620965>
 22. Kiers HAL, Krijnen WP (1991) An efficient algorithm for PARAFAC of three-way data with large numbers of observation units. *Psychometrika* 56(1):147–152. <https://doi.org/10.1007/BF02294592>
 23. Bro R, Sidiropoulos ND (1998) Least squares algorithms under unimodality and non-negativity constraints. *J Chemom* 12(4):223–247. [https://doi.org/10.1002/\(SICI\)1099-128X\(199807/08\)12:4%3C223::AID-CEM511%3E3.0.CO;2-2](https://doi.org/10.1002/(SICI)1099-128X(199807/08)12:4%3C223::AID-CEM511%3E3.0.CO;2-2)
 24. Martínez-Montes E, Sanchez JM, Valdés-Sosa P (2008) Penalized PARAFAC analysis of spontaneous EEG recordings. *Stat Sin* 18:1449–1464
 25. Estienne F, Matthijs N, Massart DL, Ricoux P, Leibovici D (2001) Multi-way modelling of high-dimensionality electroencephalographic data. *Chemom Intell Lab Syst* 58(1):59–72. [https://doi.org/10.1016/S0169-7439\(01\)00140-X](https://doi.org/10.1016/S0169-7439(01)00140-X)
 26. Kruskal JB (1989) Rank, decomposition, and uniqueness for 3-way and N-way arrays. *Multiway data analysis*. North-Holland Publishing Co, Netherlands, pp 7–18
 27. Rošťáková Z, Rosipal R, Seifpour S (2020) Tucker tensor decomposition of multi-session EEG data. In: Farkaš I, Masulli P, Wermter S (eds) *Artificial neural networks and machine learning - ICANN 2020*. Springer, Switzerland, pp 115–126. https://doi.org/10.1007/978-3-030-61609-0_10
 28. Ester M, Kriegel H-P, Sander J, Xu X (1996) A density-based algorithm for discovering clusters in large spatial databases with noise. In: *Second international conference on knowledge discovery & data mining*, pp 226–231. AAAI Press, USA
 29. Yokota T, Cichocki A (2014) Multilinear tensor rank estimation via Sparse Tucker Decomposition. In: *Joint 7th international conference on soft computing and intelligent systems (SCIS) and 15th International Symposium on Advanced Intelligent Systems (ISIS)*, pp 478–483. <https://doi.org/10.1109/SCIS-ISIS.2014.7044685>
 30. Cohen MX (2017) Comparison of linear spatial filters for identifying oscillatory activity in multichannel data. *J Neurosci Methods* 278:1–12. <https://doi.org/10.1016/j.jneumeth.2016.12.016>
 31. He BJ (2014) Scale-free brain activity: past, present, and future. *Trends Cogn Sci* 18(9):480–487. <https://doi.org/10.1016/j.tics.2014.04.003>
 32. Tadel F, Baillet S, Mosher JC, Pantazis D, Leahy RM (2011) Brainstorm: a user-friendly application for MEG/EEG analysis. *Comput Intell Neurosci*. <https://doi.org/10.1155/2011/879716>
 33. The Mathworks, Inc.: MATLAB Version 9.10.0.1684407 (R2021a). Natick, Massachusetts (2021)
 34. Wen H, Liu Z (2016) Separating fractal and oscillatory components in the power spectrum of neurophysiological signal. *Brain Topogr* 29(1):13–26. <https://doi.org/10.1007/s10548-015-0448-0>
 35. Tucker LR (1966) Some mathematical notes on three-mode factor analysis. *Psychometrika* 31(3):279–311. <https://doi.org/10.1007/BF02289464>